doi:10.1016/j.jmb.2008.09.017 J. Mol. Biol. (2008) 384, 422–435

JMB

Available online at www.sciencedirect.com

ScienceDirect

ELSEVIER

Histidine Kinase Regulation by a Cyclophilin-like Inhibitor

David A. Jacques[1], David B. Langley[1], Cy M. Jeffries[1], Katherine A. Cunningham[2], William F. Burkholder[2], J. Mitchell Guss[1] and Jill Trewhella[1]*

[1]*School of Molecular and Microbial Biosciences, University of Sydney, Sydney, New South Wales 2006, Australia*

[2]*Department of Biological Sciences, Stanford University, 371 Serra Mall, Stanford, CA 94305, USA*

Received 6 August 2008; received in revised form 9 September 2008; accepted 10 September 2008
Available online 16 September 2008

Edited by K. Morikawa

The sensor histidine kinase A (KinA) from *Bacillus subtilis* triggers a phosphorelay that activates sporulation. The antikinase KipI prevents sporulation by binding KinA and inhibiting the autophosphorylation reaction. Using neutron contrast variation, mutagenesis, and fluorescence data, we show that two KipI monomers bind via their C-domains at a conserved proline in the KinA dimerization and histidine-phosphotransfer (DHp) domain. Our crystal structure of the KipI C-domain reveals the binding motif has a distinctive hydrophobic groove formed by a five-stranded antiparallel β-sheet; a characteristic of the cyclophilin family of proteins that bind prolines and often act as *cis–trans* peptidyl-prolyl isomerases. We propose that the DHp domain of KinA transmits conformational signals to regulate kinase activity via this proline-mediated interaction. Given that both KinA and KipI homologues are widespread in the bacterial kingdom, this mechanism has broad significance in bacterial signal transduction.

Keywords: bacterial signal transduction; cyclophilin; histidine kinase inhibition; small-angle scattering; neutron contrast variation

Introduction

Sensor histidine kinases are used by bacteria, fungi, and plants in signaling pathways to detect diverse environmental signals and orchestrate adaptive responses such as chemotaxis, virulence, antibiotic resistance, metabolite utilization, and development.[1] Cells of the bacterium *Bacillus subtilis* can develop into spores in response to depleted nutrients, and the initiation of sporulation is regulated primarily by histidine kinase A (KinA). Autophosphorylation of KinA triggers a phosphorelay whereby the phosphate is transferred from KinA via the phosphotransfer proteins Spo0F and Spo0B to the response regulator Spo0A; a transcription factor that directly controls the expression of more than 120 genes involved in spore development.[2–4]

Like all known histidine kinases, the sensor function of KinA is localized in its N-terminal domains that communicate a yet to be identified environmental signal to the C-terminal autokinase. The KinA autokinase (from here on referred to as KinA$^{383–606}$) can be overexpressed as a functional enzyme[5] and is composed of a dimerization and histidine phosphotransfer (DHp) domain and a catalytic and ATP-binding (CA) domain (Fig. 1a).[8] The KinA$^{383–606}$ sequence is homologous to the histidine kinase HK853 from *Thermotoga maritima* for which there is a crystal structure [protein data bank (PDB) entry 2C2A].[9] Our previous small-angle scattering studies[6] confirmed that the KinA$^{383–606}$ dimer (KinA$_2$) has the same distinctive shape of HK853 with its globular CA domains positioned symmetrically either side of the four-helix bundle formed by the dimerizing DHp domains, referred to as the 'stalk.' The DHp stalk carries the histidines (H405, one from each subunit) that are phosphorylated upon KinA activation. The γ-phosphate of ATP is delivered by the CA domain to the histidine of the partner subunit, likely involving movement of the CA domain toward the DHp domain facilitated by a flexible linker between them.

There are many control points in the pathways that regulate spore formation in *B. subtilis*, including at the level of transcription of the phosphorelay

*Corresponding author. E-mail address: jtrewhella@usyd.edu.au.

Abbreviations used: KinA, histidine kinase A; DHp, dimerization and histidine phosphotransfer; CA, catalytic and ATP-binding; KipI, kinase inhibitor protein; Sda, suppressor of *dnaA*; GST, glutathione *S*-transferase; AI-2, autoinducer-2; TCEP, tris(2-carboxyethyl)-phosphine hydrochloride.

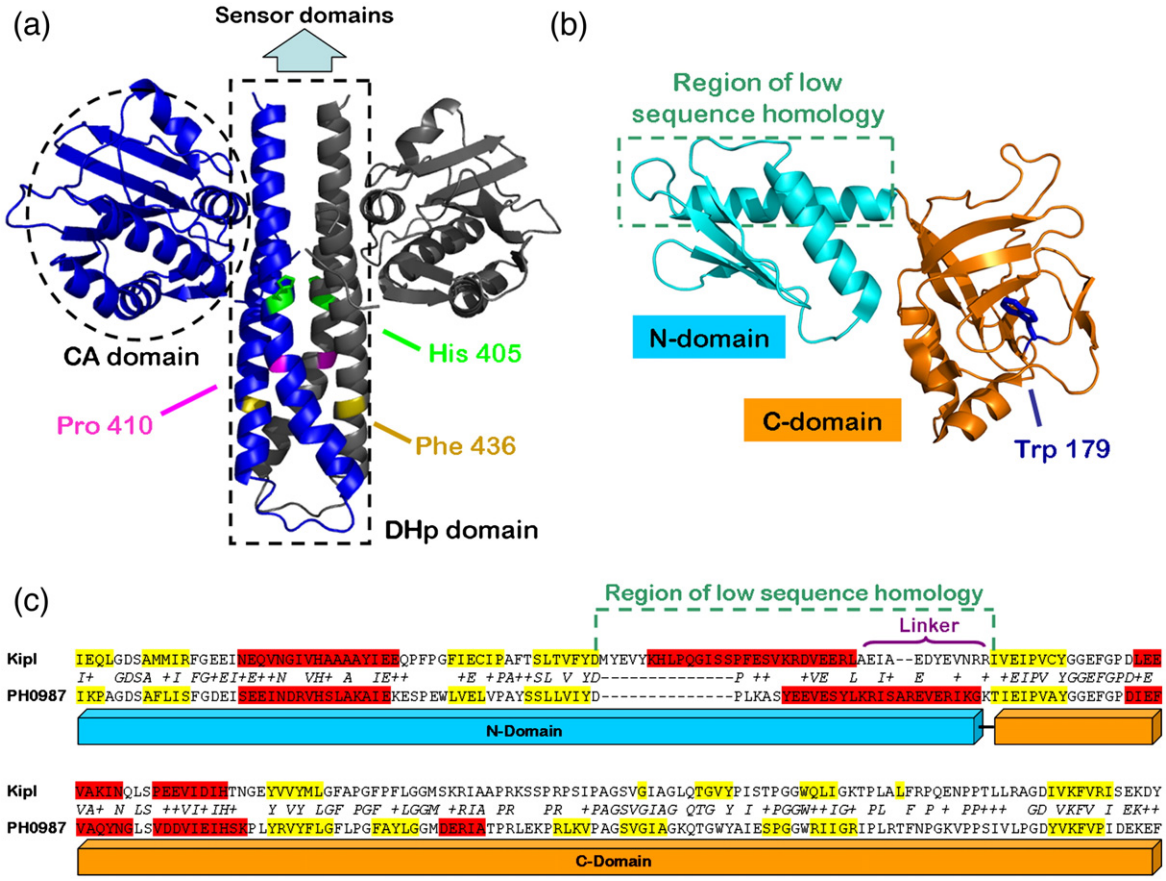

Fig. 1. KinA$^{383–606}$ and KipI homology models. (a) KinA$_2$ homology model from the previously published KinA$_2$–2Sda structure, based on the crystal structure of HK853 with the positions and orientations of the CA and DHp domains refined against the scattering data for that complex.[6] Positions of key residues H405, P410, and F436 (corresponding to H260, P265, I296 in HK853) are indicated. (b) The crystal structure of the KipI homologue PH0987 (PDB entry 2PHC) comprising an N-terminal domain (cyan) and a C-terminal domain (orange) separated by a short linker sequence. W179 (corresponding to W195 in KipI) is shown as blue sticks. (c) Sequence alignment of *B. subtilis* KipI with PH0987 from *P. horikoshii*. Identical residues are indicated in italics and '+' indicates similar residues. Secondary structural elements identified from the crystal structure in the case of PH0987 and predicted for KipI (using JPRED[7]) are colored red (α-helix) and yellow (β-sheet). KipI has an additional 7% 'gap' sequence, which appears in a region of low sequence homology to PH0987.

genes, the activity of specific phosphatases targeting either Spo0F or Spo0A, and the expression of histidine kinase inhibitors.[3,10,11] Two of these kinase inhibitors, or 'antikinases,' are KipI (kinase inhibitor protein) and Sda (suppressor of *dnaA*).[12,13] KipI and Sda appear to inhibit KinA by directly binding to the autokinase domain and preventing exchange of phosphate from ATP to H405 while also preventing the reverse reaction—transfer of phosphate from H405~P to ADP. Neither KipI nor Sda prevent transfer of phosphate from H405~P to Spo0F, nor do they stimulate dephosphorylation of KinA.[5,13]

Transcription of the gene encoding Sda is upregulated when DNA replication is perturbed or DNA damage is detected,[12,14] thereby ensuring that cells complete chromosome replication before initiating spore development. The production of KipI appears to be linked to the utilization of nitrogen and many KipI sequence homologues from other organisms have been classified as putative allophanate hydrolases, although this activity has not been demonstrated for KipI.[13] The operon containing the *kipI* gene is induced by glucose when preferred nitrogen sources such as ammonia or glutamine are scarce; however, additional factors influence the activity of KipI. KipI is coexpressed with a second protein, KipA, which prevents KipI from inhibiting KinA *in vivo* and *in vitro*.[13] Cells growing in the presence of glucose and a nonpreferred nitrogen source thus appear to be poised so that an additional signal can inhibit sporulation by antagonizing KipA, leaving KipI free to inhibit KinA.

Solution NMR and mutagenesis experiments determined that Sda has an α-helical hairpin structure with an exposed hydrophobic surface that is implicated in KinA binding.[5] Our solution structure of the KinA$_2$–2Sda complex, based on neutron contrast variation data, shows two Sda monomers binding symmetrically on opposite sides of the KinA DHp stalk and toward the end that is distal to the CA domains.[6] While there is no crystal structure for KipI, the structure of a homologous protein has been solved—PH0987, a two-domain protein of unknown function from *Pyrococcus horikoshii* (PDB entry 2PHC).

Using a combination of small-angle scattering with neutron contrast variation, fluorescence, mutagenesis, and crystallography, we have determined that two KipI monomers bind to the $KinA_2$ DHp domain, each via their C-terminal domains that have a cyclophilin-like structure. Further, this interaction involves conserved proline residues (one in each KinA subunit) that sit five residues away from each autophosphorylation site of the DHp domain.[15] We propose that inhibitory signals within the DHp domain of this and other histidine kinases are regulated by recognition of the conserved proline and may involve a *cis–trans* peptidyl-prolyl isomerization.

Results

KipI has two domains and forms a homodimer via interactions between its N-terminal domains

The crystal structure of *P. horikoshii* PH0987 is shown in Fig. 1b and a sequence alignment of KipI with that of PH0987 is shown in Fig. 1c. Overall, the two proteins have 47% sequence identity (64% similarity) and we therefore expect KipI to have the same two-domain architecture as PH0987. We were successful in crystallizing and solving the structure of the KipI C-domain (see below) and found that, as predicted, it has a fold similar to that of the PH0987 C-domain. Small-angle X-ray scattering data (Fig. 2a) were used to characterize the solution structure of the full-length KipI, which size-exclusion chromatography (SEC) and dynamic light scattering indicate is a dimer. The inverse Fourier transform of the scattering data (calculated using GNOM[16]) yields the probable distribution of distances between atoms in the proteins, $P(r)$ *versus* r (Fig. 2b), along with the radius of gyration, R_g, maximum linear dimension, D_{max}, and zero-angle scattering, $I(0)$ (Table 1). $I(0)$, normalized for protein concentration (milligrams per milliliter) and molecular weight of the scattering species, is expected to be constant and our $I(0)$ analysis confirms that, like KinA, KipI forms a homodimer. The KipI dimer ($KipI_2$) is a more extended structure compared to $KinA_2$ (Table 1,

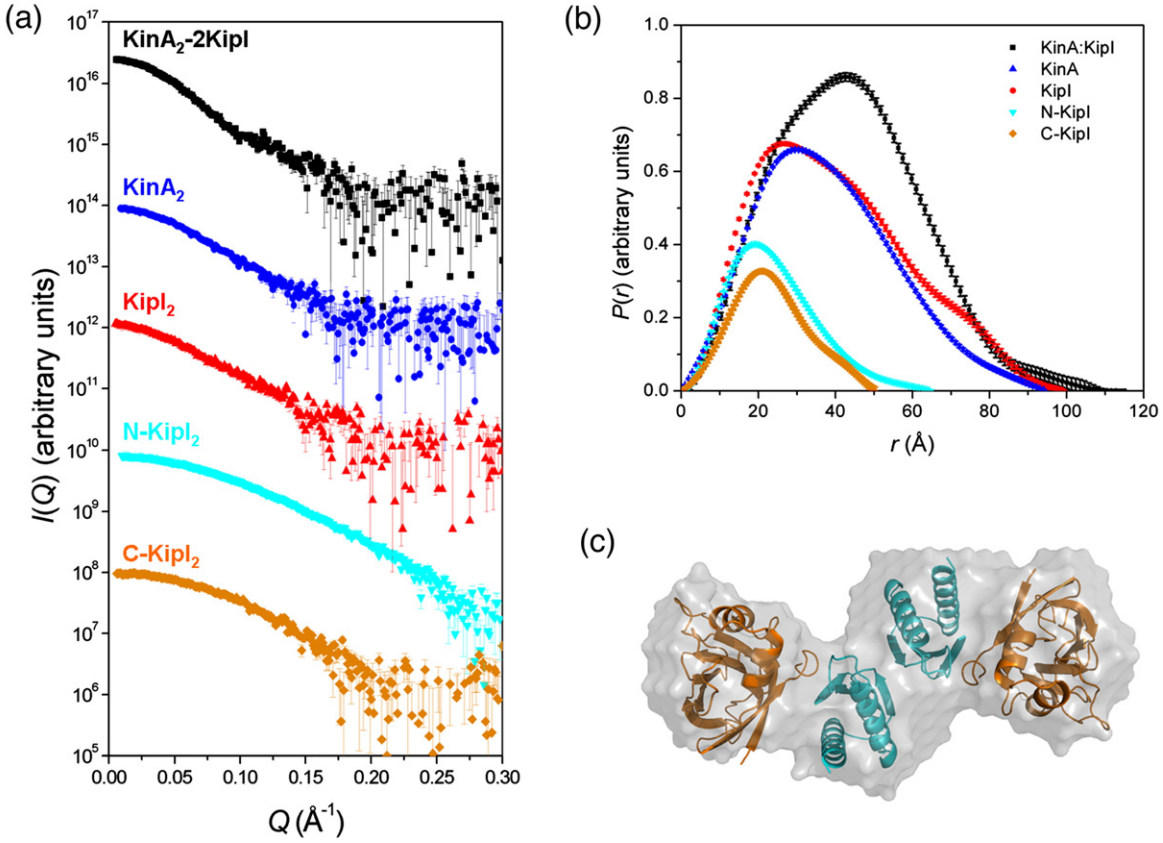

Fig. 2. X-ray scattering data for $KinA^{383–606}$, KipI, and the complex they form. (a) Solvent-blank-subtracted X-ray scattering profiles, $I(Q)$ *versus* Q, for the $KinA_2$–2KipI complex (black), for $KinA_2$ (blue), $KipI_2$ (red), and the KipI N- and C-domains (cyan and orange, respectively). The plots have been shifted on the vertical axis relative to each other for clarity. The Guinier plots corresponding to these profiles are presented in Supplementary Fig. 1 and show the expected linearity for solutions of monodisperse, identical particles. (b) $P(r)$ *versus* r calculated as the indirect Fourier transforms of the scattering data for the $KinA_2$–2KipI complex, $KinA_2$, $KipI_2$, and the N- and C-domains [colored as in (a)]. The $P(r)$ curves are scaled (by × 3 for $KinA_2$ and $KipI_2$, and ×4.6 and ×8 for the N- and C-domains) so that the features of the curves can be seen. (c) The best-fit KipI dimer structure optimized using rigid-body refinement. The model is superimposed in the molecular envelop determined by *ab initio* shape restoration from the scattering data.

Table 1. Structural parameters derived from the scattering data

X-ray scattering data from the individual proteins and their complex

Protein/Complex	Protein conc. (mg/mL)	$(I(0)/c/MW)^a$	R_g (Å)	D_{max} (Å)
$KipI_2$	4.0	1.03	31.3±0.2	100
KipI N-domain	11.2	0.97	18.55±0.02	60
KipI C-domain	1.6	0.97	17.94±0.08	58
$KinA_2$	3.7	1.00	29.6±0.1	95
$KinA_2$–2^DKipI	5.3	1.02	33.4±0.2	100

Neutron scattering data from the $KinA_2$–2KipI complex

Component	Stuhrmann analysis, R_g (Å)[b]	Component scattering functions	
		R_g (Å)	D_{max} (Å)
$KinA_2$	26.0±0.9	24.9±0.2[c]	78[c]
2^DKipI	34.0±0.9	34.5±0.5	115

[a] These values have been normalized to the corresponding ratio for lysozyme and assume KinA and KipI are dimers alone and are in a 2:2 stoichiometry when complexed. Combined statistical errors in $I(0)$ values are <1%, while the uncertainty in protein concentrations must be <5% based on the excellent agreement of the normalized experimental $I(0)/c/MW$ values with the expected value of 1.0. Protein concentrations for the neutron scattering experiments were 5.3 mg/mL.

[b] The Stuhrmann plot and quadratic fit used to determine structural parameters are shown in Supplemental Fig. 2. The separation of centers of mass of the deuterated and nondeuterated components determined from the fit is 17±8 Å.

[c] For $KinA_2$ in the $KinA_2$–2Sda complex, R_g=25.2±0.1 Å, D_{max}=75 Å.[9]

Fig. 2b) and *ab initio* shape restoration calculations from the scattering data yield a molecular envelope that has one dimension much longer than the other two (Fig. 2c). A symmetric KipI dimer was created based on the crystal structure of PH0987 and the positions and orientations of the subunits were optimized by rigid-body refinement against the KipI scattering data. The N- and C-domains were allowed to move independently in the refinement to account for possible differences in the low-sequence-homology region linking the domains (Fig. 1b and c). As multiple refinements did not discriminate between the dimer interactions involving the N- or C-terminal domains, we measured scattering data for the N- and C-domains alone (Table 1, Fig. 2a), each prepared freshly and maintained under strongly reducing conditions to inhibit disulfide formation. The $I(0)$ analysis, along with the R_g and D_{max} values derived from $P(r)$, show that the C-domain in solution is a monomer, while the smaller N-domain forms a dimer. The KipI dimer model shown in Fig. 2c, superposed with the molecular envelope from shape restoration, has the N-domains interacting and is the model that best fits the scattering data (Fig. 2a) from 20 independent rigid-body refinements. The χ value for the fit is 1.6, indicating a reasonable but not ideal fit, possibly due to flexibility in the longer domain linker in KipI compared to PH0987.

Two KipI monomers bind symmetrically to the $KinA_2$ DHp domain to form a $KinA_2$–2KipI complex

Size-exclusion chromatography of an equimolar mixture of KipI and $KinA^{383–606}$ yielded an early-eluting peak that SDS-PAGE and amino acid analysis determined to contain both proteins in approximately equimolar amounts. Dynamic light scattering gave a single peak corresponding to a molecular mass of ~112 kDa and $I(0)$ analysis of the scattering data confirmed this value (Table 1). Thus, all indicators are that KipI forms a tight complex with $KinA^{383–606}$ in a 2:2 stoichiometry. We used small-angle neutron contrast variation to determine the nature of this complex, similar to our previous work on the $KinA_2$–2^DSda complex.[6]

The intensity of the scattering signal from a protein depends on the difference between its scattering density and that of its solvent (the 'contrast') and the scattering density of a protein and its solvent can be systematically manipulated by substitution of hydrogen ($^1H \equiv H$) for deuterium ($^2H \equiv D$). Neutron scattering data obtained from a complex containing deuterated and nondeuterated proteins in solvents with different H_2O/D_2O ratios constitute a contrast series from which structural parameters for the proteins and their relative dispositions can be obtained. Neutron scattering profiles were measured for $KinA^{383–606}$ complexed with deuterated KipI (^{D}KipI) in 0%, 10%, 20%, 30%, 40%, 80%, 90%, and 100% D_2O (Fig. 3a). The KipI deuteration level (61%) was chosen so that high-contrast data could be collected either side of the solvent match point for the total particle (63% D_2O), thus maximizing the information content in the contrast series on the deuterated and nondeuterated components. The relationship between the observed R_g value and the inverse of the mean contrast of the complex yields R_g estimates for the $KinA^{383–606}$ and ^{D}KipI components within the complex as well as the approximate separation of their centers of mass[17] (Table 1). Analysis of the neutron contrast series data in terms of the component scattering functions yields the individual scattering profiles for dimeric $KinA^{383–606}$ and bound ^{D}KipI monomers as well as the 'cross-term' that contains information about their relative dispositions within the complex.[17] These component scattering functions and their respective $P(r)$ profiles are shown in Fig. 3b and c, while Table 1 gives the associated R_g and D_{max} values. The structural parameters obtained from the different analyses of the neutron contrast series are the same within experimental error, demonstrating that the data are of the high quality needed for accurate structural interpretation. Of note, the significantly larger R_g value for KipI in the complex compared to that for the KipI dimer in solution indicates that the two KipI monomers are well separated in the complex.

As we observed for Sda, KipI binding affects the structure of $KinA_2$. The structural parameters for the $KinA_2$ component of the complex with ^{D}KipI are identical (within experimental error) to those

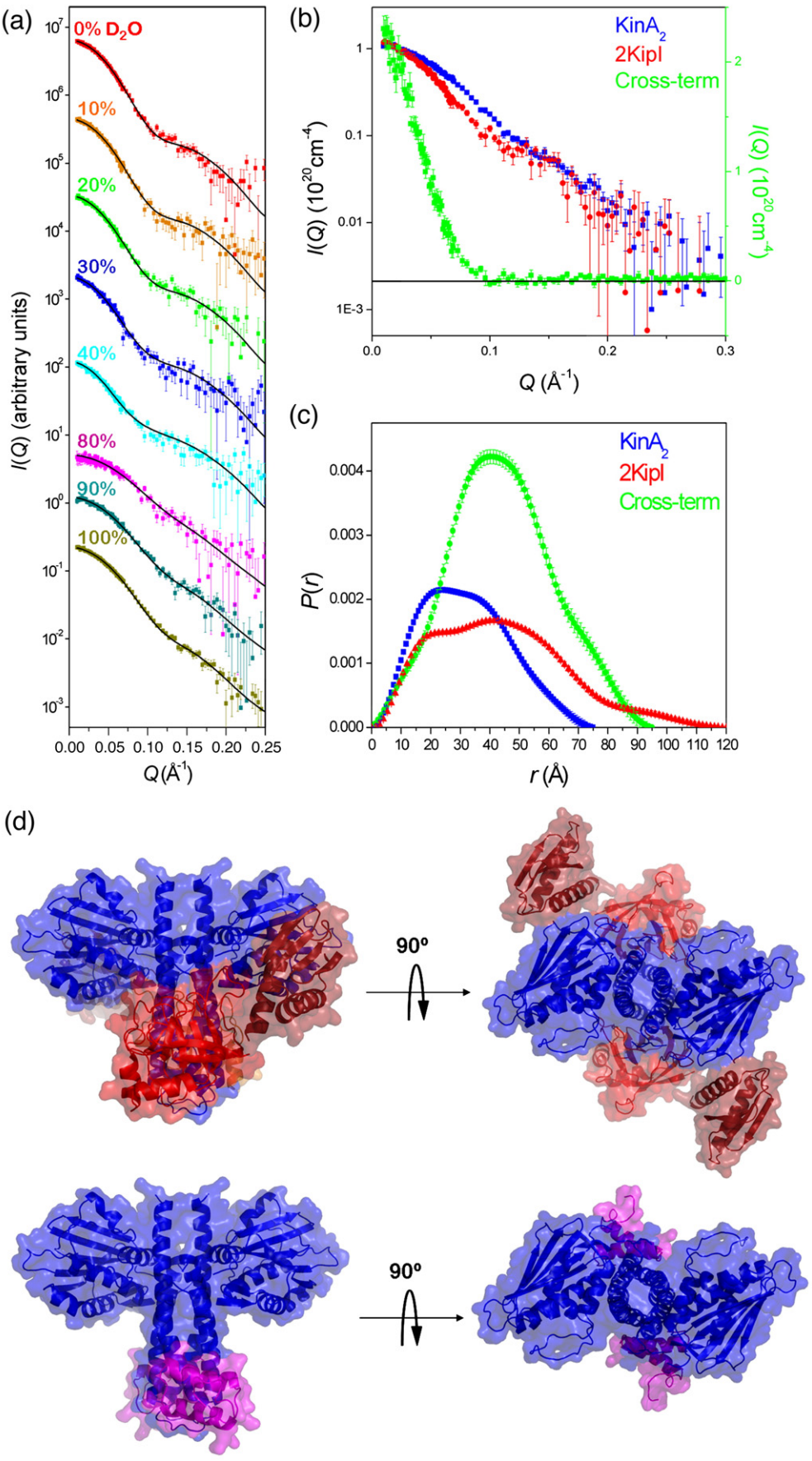

Fig. 3 (*legend on next page*)

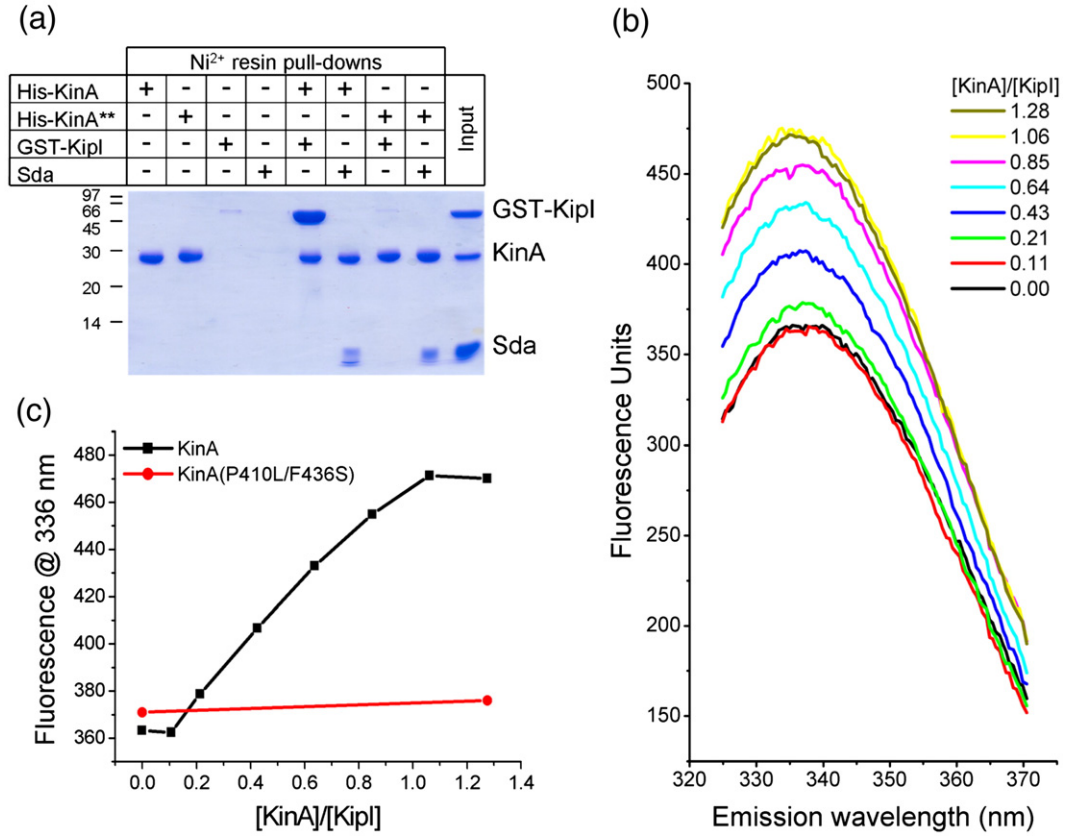

Fig. 4. The DHp domain of KinA binds the C-domain of KipI. (a) SDS-PAGE showing the results of Ni^{2+}-pull-down assays. Wild-type $KinA^{383–606}$ binds GST-KipI and Sda, while the $KinA^{383–606}$(P410L/F436S) mutant retains the ability to bind Sda but not KipI. (b) The fluorescence signal from W195 in KipI increases as $KinA^{383–606}$ binds, indicating that the environment of this residue changes as the complex forms. (c) In contrast to the results for wild-type $KinA^{383–606}$ (black trace), the fluorescence signal does not change when $KinA^{383–606}$(P410L/F436S) is titrated with KipI (red trace).

derived for $KinA_2$ in the $KinA_2$–2^{D}Sda complex (Table 1), indicating that both inhibitors induce a similar overall compaction of $KinA_2$. To build a starting model for rigid-body refinement against the neutron scattering data, we therefore used the $KinA_2$ homology model that has already been refined to best fit the scattering data in our $KinA_2$–2^{D}Sda study (Fig. 1a). For the KipI component we used the crystal structure of PH0987, allowing the N- and C-domains to move independently as was done for the KipI dimer modeling (above). Multiple independent rigid-body refinements yielded models that consistently placed the KipI C-domains in contact with the DHp domain of $KinA_2$, while the KipI N-domains showed either no interaction or a small surface area interaction with the CA domains. Our best-fit model is shown in Fig. 3d (top), with the corresponding fits to the experimental data in Fig. 3a (black curves). This model gives near-ideal χ^2 values against the neutron scattering data (0.96, 0.86, 0.83, 0.98, 1.10, 1.02, 0.90, and 0.99 for the 0%, 10%, 20%, 30%, 40%, 80%, 90%, and 100% D_2O data, respectively) with no steric clashes between the components. Our previously determined $KinA_2$–2Sda model is shown for comparison (Fig. 3d, bottom).

The $KinA_2$–2KipI interaction involves proline 410 in the KinA DHp domain and tryptophan 195 in the KipI C-domain

We used pull-down assays and tryptophan fluorescence experiments with native $KinA^{383–606}$ and the double mutant $KinA^{383–606}$(P410L/F436S) to identify specific residues at the KinA–KipI interface. In addition to the interactions suggested by our neutron-derived model for the complex, mutational analysis

Fig. 3. Neutron contrast variation data for $KinA_2$–2KipI and best-fit models for the $KinA_2$–2KipI and $KinA_2$–2Sda complexes. (a) Neutron scattering profiles, $I(Q)$ *versus* Q, measured for the contrast variation series overlaid with the model profiles for the best-fit model of the complex shown in (d). (b) Component scattering functions corresponding to the scattering profiles for $KinA_2$ the two bound ^{D}KipI subunits, and the cross-term between them. (c) $P(r)$ *versus* r profiles calculated as the indirect Fourier transform of the component scattering functions in (b). (d) Top: best-fit model for the $KinA_2$–2KipI complex calculated using rigid-body refinement. The primary interaction is between the DHp domain of KinA and the C-domain of KipI. Bottom: our previously published model for $KinA_2$–2Sda[6] is shown for comparison. $KinA^{383–606}$ is shown in blue, the C-domain of KipI in red, the N-domain of KipI in dark red, and Sda in magenta).

of KinA together with protection and cross-linking studies indicate that P410, a highly conserved proline within the histidine kinase family,[15] is close to the Sda-binding site, involved in the binding of KipI, and important for inhibition by both Sda and KipI (K.A.C. and W.F.B., in preparation). P410 is located directly below H405 in the DHp domain of $KinA_2$, while F436 is positioned nearby on the adjacent helix (see Fig. 1a). The $KinA^{383–606}$(P410L/F436S) double mutant was used for experiments described here because it retains full kinase activity and is more stable in solution for biophysical and biochemical studies than the single P410L mutant (K.A.C. and W.F.B., in preparation). In performing pull-down assays, we immobilized His-tagged $KinA^{383–606}$ or $KinA^{383–606}$(P410L/F436S) on Ni^{2+} agarose beads and used them to capture Sda or glutathione *S*-transferase (GST)-tagged KipI. Use of GST-tagged KipI ensured sufficient separation between the $KinA^{383–606}$ and KipI bands on SDS-PAGE. Results show that under conditions of excess inhibitor, both the wild-type and mutant $KinA^{383–606}$ pull down Sda, but only the wild-type $KinA^{383–606}$ pulls down KipI (Fig. 4a), indicating that P410 is likely to be required for KipI binding.

The interaction of $KinA^{383–606}$ with KipI was further examined by monitoring the intrinsic fluorescence of W195, the sole tryptophan in KipI, as a function of $KinA^{383–606}$ binding. As $KinA^{383–606}$ lacks a tryptophan, changes in tryptophan fluorescence specifically probe the environment of W195. In concert with the incremental introduction of $KinA^{383–606}$ to solutions of KipI, the intensity of the tryptophan fluorescence emission peak (336 nm) increases and saturates at an approximately equimolar ratio of $KinA^{383–606}$ to KipI (Fig. 4b and c). The increased intensity of the emission peak indicates that the environment of W195 changes upon complex formation. When repeated with $KinA^{383–606}$

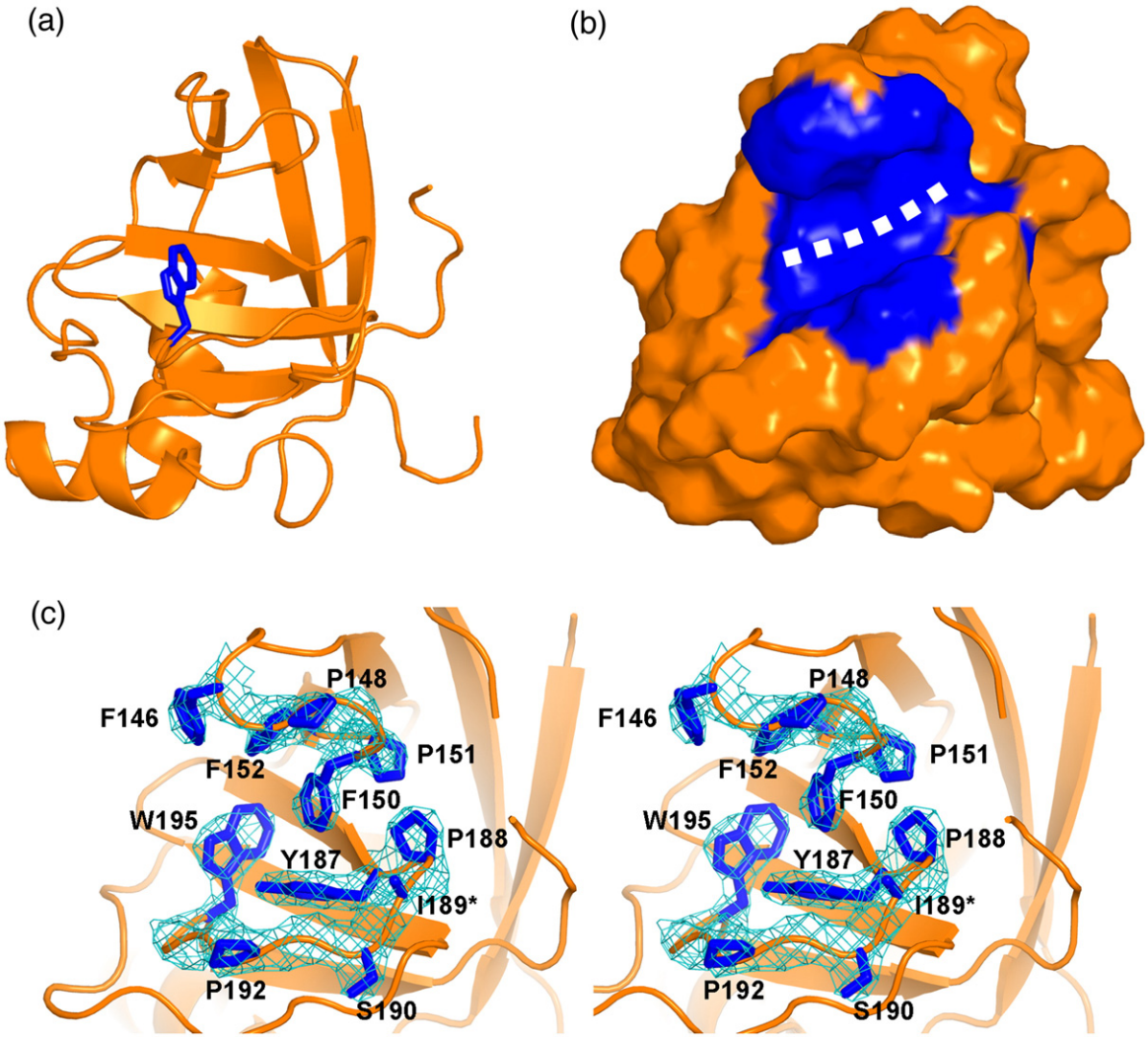

Fig. 5. Crystal structure of the C-domain of KipI. (a) Ribbon representation of the C-domain of KipI with W195 shown as sticks. (b) Surface representation of the C-domain in the identical perspective as in (a). Conserved aromatic residues forming a hydrophobic groove (dashed line) on the surface of the protein are colored blue. (c) Stereo view of the residues that form the hydrophobic groove on the surface of the C-domain. Electron density ($2F_{obs}-F_{calc}$, contoured at 1.5σ) is shown as pale blue mesh and clearly defines the aromatic residues (sticks) that are conserved in this region. *Side-chain density is absent for I189, which is truncated at C^{β}.

(P410L/F436S), there is no change in the fluorescence signal, consistent with the pull-down results with GST–KipI. These pull-down and fluorescence data confirm that the primary KinA–KipI interface involves the conserved tryptophan, W195, in the C-domain of KipI and the conserved proline, P410, of the KinA DHp domain.

The C-domain of KipI resembles a peptidyl-prolyl isomerase, whilst the N-domain resembles the quorum-sensing enzyme LuxS

We have solved the crystal structure for the KipI C-domain to 3 Å resolution (Fig. 5). Data collection and refinement statistics are given in Table 2. The structure confirms that the overall fold (Fig. 5a) is very close to that predicted from the *P. horikoshii* structure, containing two short α-helices and a five-stranded antiparallel β-sheet. The β-sheet segment defines a concave surface that includes a hydrophobic groove (Fig. 5b and c). A VAST[18] structural homology search reveals that the proteins with the highest structural similarity to the C-domain of KipI are those of the cyclophilin family (VAST rmsd, 2.1–3.1 Å for 13 structures with greater than 50% aligned sequence; Fig. 6a). Cyclophilins are a ubiquitous family of proteins whose functions include protein folding, transport, and signaling.[19] Their primary activity appears to be to catalyze the *cis–trans* isomerization of peptide bonds preceding proline residues, although there are examples of peptidyl-prolyl isomerases that can inhibit kinase activity by binding an essential proline without inducing an isomerization (e.g., FKBP12[20]). The mechanism of the peptidyl-prolyl isomerization reaction remains controversial and it has even been suggested that these enzymes need only display a hydrophobic cavity of the correct conformation to confer activity.[21] Even at the modest resolution (3 Å) of our crystal structure the electron density is well defined for the aromatic residues W195, Y187, F152, F150, and F147 as well as for the numerous proline residues that combine to define such a groove (Fig. 5c).

The structures of the full-length KipI or its N-domain have not yet been solved. However, a VAST structural homology search using the N-terminal domain of *P. horikoshii* PH0987 reveals it to be a structural homologue of the *S*-ribosylhomocysteinase (LuxS) family, (VAST rmsd 2.5–2.8 Å for 18 structures with greater than 88% sequence aligned; Fig. 6b). LuxS is an enzyme involved in producing autoinducer-2 (AI-2), a small bacterial signal molecule used in quorum sensing.[22] Of note, like the KipI N-domain, LuxS forms a dimer.

Table 2. Crystal structure data collection and refinement statistics for KipI C domain

Data collection	
Space group	$P2_12_12_1$
Cell dimensions; *a*, *b*, *c* (Å)	44.91, 84.42, 84.41
Resolution (Å)	16.88–3.01 (3.06–3.01)[a]
R_{merge}	0.14 (0.66)
Average $I/\sigma I$	6.7 (1.5)
Completeness (%)	99.8 (98.4)
Redundancy	6.0 (4.6)
Refinement	
Resolution (Å)	16.88–3.01
No. of reflections	6375
R_{work}/R_{free}	0.26, 0.34
Molecules per asymmetric unit	2
No. of nonhydrogen atoms	1635
Residues missing in residue range 100–240	A chain: 147–148, 205–213, 232–240; B chain: 207–215, 232–240
No. of residues truncated to C^{β}	A chain, 24; B chain, 29
Mean *B*-factor	37.7
rmsd	
Bond lengths (Å)	0.009
Bond angles (°)	1.2
PDB entry	2ZP2

[a] Values in parentheses are for the highest-resolution shell (of 20).

Discussion

Similarities and differences between the interactions of KinA with KipI and Sda

We previously suggested that Sda binding to the DHp domains of KinA transmits an inhibitory signal to the CA domains allosterically via some kind of conformational change.[6] Our low-resolution solution structure of $KinA_2$–2Sda has the Sda molecules toward the base of the DHp stalk in a position that appears unlikely to form a steric barrier between the CA domains and their target histidines, H405 (Fig. 3d, bottom). The KipI C-domain is approximately three times the size of Sda, and our $KinA_2$–2KipI structure shows it also interacts with the DHp domain (Fig. 3d, top). The binding interface on $KinA_2$ overlaps with that of the Sda molecules but is significantly larger, extending further toward H405. While H405 appears likely to remain exposed, the more extensive interface with the KipI C-domain plus the positioning of the N-domain as modeled would almost certainly act as a steric block, restricting the CA domains from accessing H405. In the light of the apparent differences in potential for these kinds of steric restrictions, it is interesting to note that the solution scattering data show that Sda and KipI binding induce the same overall compaction of $KinA_2$ involving a movement of the CA domains toward the DHp domain. It thus appears that the binding of either antikinase to the DHp domain induces a similar conformational signal that results in the movement of the CA domains, presumably transmitted via the four-helix bundle of the DHp domain and sequences linking to the CA domains.

The more extensive interface between $KinA_2$ and the KipI C-domain in our structural model includes the conserved proline of KinA, P410 (see Fig. 1a). The P410L/F436S mutant of $KinA^{383–606}$ was originally identified as retaining full kinase activity, yet being

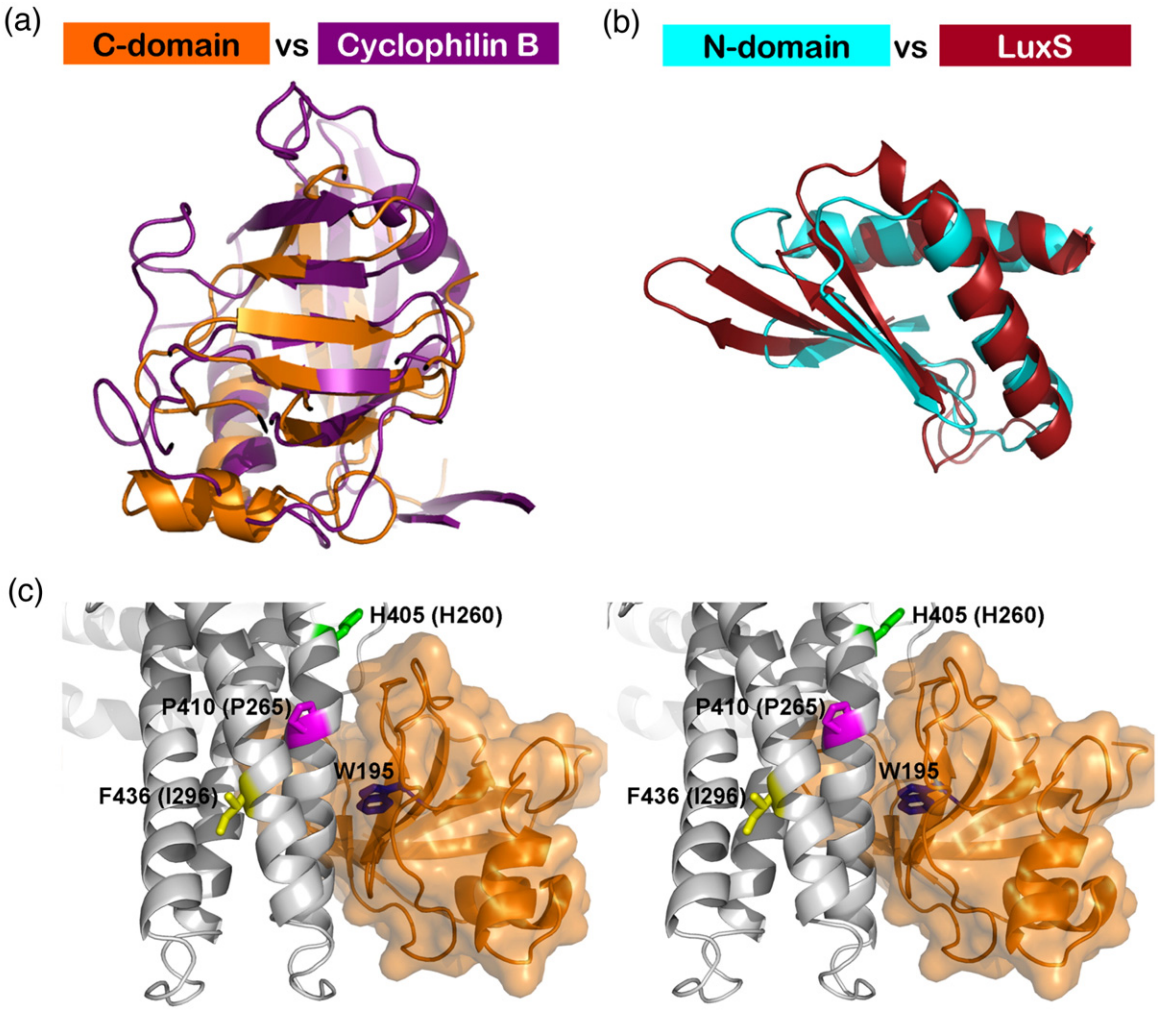

Fig. 6. Comparison of the PH0987 N- and KipI C-domains with structural homologues of known function and modeling the DHp–KipI interface. (a) Superposition of the C-domain of KipI (orange, PDB entry 2ZP2) with cyclophilin B from *Homo sapiens* (purple, PDB entry 1CYN); rmsd of 2.8 Å for 54% C^{α} alignment. The active site of cyclophilin B and the hydrophobic groove of the C-domain of KipI occur on the same five-stranded β-sheet. (b) Superposition of the N-domain of PH0987 (cyan) with the core of LuxS from *B. subtilis* (red-brown, PDB entry 2FQO); rmsd of 3.0 Å for 87% C^{α} alignment. (c) Stereo view of the proposed interaction surface between the DHp stalk of KinA (silver, based on the kinase model HK853, PDB entry 2C2A) and the C-domain of KipI (orange, PDB entry 2ZP2). Our crystal structure of the C-domain has been superposed on the C-domain of the *P. horikoshii* homologue from our neutron-scattering-derived model for the $KinA_2$–2KipI complex. The DHp residues are labeled according to their position in KinA with their corresponding positions in HK853 shown in parentheses. The conserved proline, P410, is juxtaposed against the hydrophobic groove of the C-domain containing W195. F436 is predicted to occur in the dimer interface away from the KipI binding site, while H405 is positioned just above the C-domain.

resistant to inhibition by the overexpression of Sda *in vivo* (K.A.C. and W.F.B., in preparation). Neither P410 nor F436 was predicted to interact with Sda in our previous work (P410 occurring further up the DHp stalk, and F436 being buried at the dimer interface; see Fig. 6c). Our pull-down data show that the $KinA^{383–606}$ double mutant is unable to interact with KipI, whilst still being able to bind Sda. These observations, in light of the $KinA^{383–606}$ double mutant being resistant to Sda *in vivo*, support the idea that Sda inhibits KinA via an allosteric mechanism involving a conformational change in the DHp domain and not simply through a steric blocking mechanism. In contrast, KipI binding appears to require P410. *In vivo* studies (K.A.C. and W.F.B., in preparation) have shown that the single P410L mutation, while resulting in an approximately 50% loss in sporulation frequency, is relatively unaffected by overexpression of KipI, further implicating this residue as key to KipI binding and inhibition.

KipI and Sda share no sequence or structural homology, and so differences in their interactions with KinA are not surprising. It has been suggested that while Sda can inhibit both KinA-dependent sporulation as well as the activity of the auxiliary sporulation kinase, KinB,[12] KipI only inhibits KinA-dependent sporulation.[13] The region of the hairpin in the DHp domain of KinA shares little sequence homology with KinB, and it is conceivable that some of these residues play a role in conferring specificity

for KipI. It is possible, therefore, that the different binding properties observed may reflect the different antikinase specificities of KipI and Sda.

The DHp domain and modulation of conformational signaling

Our crystal structure of the KipI C-domain reveals an overall fold and hydrophobic groove that is characteristic of the proline-binding site in the cyclophilin protein family (Fig. 6a). The aromatic residues (W195, Y187, F152, F150, F146) that define this groove in KipI are highly conserved among ~300 sequences of KipI homologues across species. An alignment of this crystal structure with the C-domain of the *P. horikoshii* homologue in our neutron-scattering-derived model for $KinA_2$–2KipI shows this groove interacting with the DHp helix carrying P410 (Fig. 6c). Based on the homology of $KinA^{383–606}$ with the histidine kinase HK853, we expect that P410 induces a bend in this helix (Figs. 1a and 6c). A similar bend is observed in the structure of the dimerization domain of the *Escherichia coli* histidine kinase, EnvZ (at P248, PDB entry 1JOY[23]). The bend allows the two helices of one monomer to pack more tightly against the two helices of the partner monomer, resulting in a tightly twisted four-helix bundle. A protein that is structurally similar to $KinA^{383–606}$ but does not have a proline in this position is the phosphotransfer protein Spo0B (PDB entry 1IXM[24]) whose four-helical bundle is less tightly wound compared to the other structures. Distinct from the histidine kinases, Spo0B has no autokinase activity and, as such, the differences between their DHp domains may reflect the nature of different conformational requirements for function. By binding in the region of P410, possibly inducing cis–trans isomerization of this residue, it is likely that KipI alters the conformation of the DHp domain so that autokinase activity is inhibited.

It has been shown that neither KipI nor Sda inhibits the phosphotransfer reaction between KinA and Spo0F.[5,13] In our $KinA_2$–2Sda model,[6] we noted that some steric overlap might be expected between Sda and the Spo0F recognition site, although it is conceivable that both could be bound to $KinA^{383–606}$ at the same time. In our $KinA_2$–2KipI model, this steric overlap is far more severe and would preclude simultaneous binding of Spo0F and KipI. To account for the biochemical data in the context of these structural data, one can consider the possibility of competing equilibria allowing Spo0F transient access to the phosphorylated histidine. For instance, the autokinase activity of KinA might still be inhibited by the binding of just one KipI molecule. In such a scenario, should a single KipI molecule dissociate from one side of the DHp stalk, Spo0F could gain access to one of the target histidines. Alternatively, it is also possible that structural rearrangements in the DHp domain induced by KipI (such as cis–trans isomerization of P410) might be sustained in the DHp domain for a time after dissociation, allowing access to Spo0F while transiently inhibiting further autophosphorylation.

A possible role for antikinases in quorum sensing?

Quorum sensing in bacteria is used to regulate gene expression in response to local population density, resulting in community-wide responses such as sporulation, secretion of virulence factors, motility, and biofilm formation.[25] Interestingly, the phosphorelay governing sporulation in *B. subtilis* is also responsible for regulating biofilm development. While high levels of the transcription factor Spo0A~P triggered by KinA activity induce sporulation, low levels of Spo0A~P resulting from the activities of other sensor histidine kinases induce expression of genes associated with biofilm formation.[26] Quorum sensing and biofilm production are therefore intimately related to the *B. subtilis* sporulation phosphorelay and recently, KipI and Sda have been implicated in regulating at least one of the histidine kinases involved in biofilm formation.[27]

In light of these observations, it is intriguing that the N-domain of KipI shares structural homology with LuxS, an enzyme required for synthesis of the quorum-sensing, interspecies signaling molecule AI-2.[22] As KipI interacts with KinA via its C-domain, the N-domain is available to act as a potential sensor for small molecules or as a recognition site for other proteins. While it is known that the inhibitory effect of KipI is antagonized by interaction with KipA,[13] little is understood of the nature and regulation of this interaction. It is interesting to speculate that the actions of KipI, KipA, and possibly even AI-2 or a like molecule might combine to coordinate sporulation and biofilm development.

Conclusions

Based on our structural data on $KinA^{383–606}$ and the antikinases KipI and Sda, and comparisons with structural and functional homologues, we propose that the helix-bending P410 in the KinA DHp is targeted by the hydrophobic groove of the KipI C-domain. Whilst KipI binding at P410 appears capable of altering KinA autophosphorylation activity through steric effects alone, the similarity of the observed $KinA^{383–606}$ compaction to that caused by the much smaller Sda suggests that allosteric effects, perhaps involving isomerization of P410, play a role in the $KinA_2$–2KipI complex. It is possible that this proline, whose isomerization would dramatically affect the 'conformational twist' of the DHp, constitutes a proline-mediated switch that regulates kinase activity. Such a mechanism would have broad significance, representing a novel structural conduit for the regulation of other sensor histidine kinase signal transduction systems.

While we have focused here on the role of KipI in regulating spore formation in *B. subtilis*, it is important to note that KipI homologues are found in diverse species in the bacterial kingdom, including

gram-negative species not capable of forming spores. Indeed, *P. horikoshii*, which provided our initial KipI model, does not sporulate, indicating that the role of KipI is more extensive than simply being an inhibitor of endospore formation. The homology it shares with proteins associated with quorum sensing supports this idea. The possibility that KipI and its homologues in other species have roles involved in environmental sensing, bacterial communication, and orchestrated multicellular development presents an exciting new dimension to this family of proteins.

Materials and Methods

Cloning

The full-length KipI gene and segments encoding the predicted N- and C-terminal domains (residues 1–99 and 100–240, respectively) were PCR amplified from *B. subtilis* chromosomal DNA (laboratory strain 168). Oligonucleotide primers (Geneworks, Australia) and plasmid construct details are given in Supplementary Table 1. Both N-terminal His- and N-terminal GST-tagged versions of the full-length protein were produced, whilst the N- and C-terminal domains were produced as N-His-tag fusions only. Expression tags were removable using thrombin.

Protein overexpression and purification

The autokinase domain of *B. subtilis* KinA (residues 383–606) and full-length Sda were overexpressed and purified as described previously.[6] The KinA$^{383–606}$ (P410L/F436S) mutant was overexpressed from a pET28b-based plasmid pKC20 and purified as per the wild-type. The KipI full-length N- and C-domain constructs were overexpressed in *E. coli* BL21(DE3) grown in LB medium (100 μg/mL ampicillin) at 30 °C, induced with 1 mM IPTG. Cells were harvested 4 h post-induction and lysed with lysozyme (~100 μg/mL) and 0.1 mM phenylmethylsulfonyl fluoride with cycles of freeze–thaw and pressure shock in Buffer A: 50 mM Tris (pH 8.5), 200 mM NaCl, and 5 mM tris(2-carboxyethyl)-phosphine hydrochloride (TCEP). Insoluble material was removed by centrifugation (50,000*g*, 1 h, 4 °C).

His-tagged or GST-tagged proteins were purified by sequential passage over DEAE-agarose and Ni-NTA® resin (imidazole elution) or DEAE-agarose and glutathione-agarose resin (glutathione elution), respectively. SEC was performed on His-tagged proteins by passage over a HiLoad® 16/60 Superdex 200 prep-grade column where isocratic elution was performed using Buffer B: 150 mM imidazole, 50 mM Tris (pH 8.5), 200 mM NaCl, 5 mM TCEP. Protein purity was judged to be >99% by SDS-PAGE. SEC of KipI yielded a major peak that dynamic light scattering showed contained a single mass as expected for dimeric 6His-tagged KipI (~58 kDa). The KipI samples ran as a monomer on nonreducing SDS-PAGE, indicating that the dimerisation is not disulfide-mediated. KinA$^{383–606}$ purified as a dimer (~54 kDa by dynamic light scattering). Storage, transport, fluorescence, and scattering experiments all used purified proteins in Buffer B.

^{D}KipI was produced by culturing cells in M9 salts minimal medium dissolved in 80% (v/v) D_2O with nondeuterated glucose. Cells were first adapted to D_2O by sequential inoculation of 50% and 80% D_2O starter cultures. Overexpression and purification of ^{D}KipI was performed as described above for KipI except due to the reduced growth rates, the cells were harvested 12 h post-induction. Tryptic peptide masses from KipI and ^{D}KipI were obtained by matrix-assisted laser desorption/ionization time-of-flight mass spectrometry (QSTAR XL Hybrid Mass Spectrometer equipped with an oMALDI source) and their difference was used to calculate the level of protein deuteration.

Protein concentrations were estimated using calculated molar extinction coefficients at 280 nm (5960 M^{-1} cm^{-1} for KinA$^{383–606}$ and 23,505 M^{-1} cm^{-1} for KipI, calculated using the ProtParam tool[28]). The $KinA_2$–2KipI complexes (including those with ^{D}KipI) were formed by incubating a 1:1 molar ratio of KinA$^{383–606}$/KipI for 30 min at room temperature. The complex was separated from any unbound components by SEC (described above) and quantitative amino acid analysis, to confirm the stoichiometry, was performed at the University of Utah with an L-8800 Hitachi AAA instrument.

Small-angle scattering

Samples used for X-ray scattering were dialyzed overnight against Buffer B and the dialysate was used for solvent blank measurements. Samples of the complex for neutron scattering experiments were dialyzed against Buffer B with D_2O concentrations of 0%, 10%, 20%, 30%, 40%, 80%, 90%, and 100% (v/v) and the respective dialysates were used as solvent blanks. The monodispersity of samples for scattering was confirmed by dynamic light scattering and by comparison to the scattering of a lysozyme standard known to be monodisperse.[29] This comparison also confirms that there were no correlated interparticle distances, and therefore the samples approximated infinite dilution conditions for scattering. The absence of interparticle interference was further confirmed in the neutron experiments by placing the data on an absolute scale and thereby allowing the molecular weight of the complex to be calculated for each contrast point.[30] The average molecular mass obtained from six high-contrast measurements is 114 kDa with a standard deviation of 5, in excellent agreement with the expected value based on amino acid composition (112 kDa). The good agreement of these values between contrast points confirms that the stoichiometry of the complex in our samples is 2:2.

X-ray scattering measurements were performed with an Anton Paar SAXSess with line collimation and CCD detector as described previously.[31] Protein samples and their solvent blanks in a 1-mm capillary were each exposed for 60 min at 10 °C with the use of a 10-mm slit and 10-mm integration width. Solvent subtractions and data reduction to $I(Q)$ *versus* Q (where $Q=(4\pi \sin\theta)/\lambda$, where 2θ is the scattering angle and $\lambda=1.54$ Å, the wavelength of the radiation) were done using SAXSquant1D (Anton-Paar, Austria). Neutron scattering data were collected with the use of NG3[32] at the National Institute for Standards and Technology at 20.0 °C in 1-mm path-length Hellma quartz cylindrical cells and using a neutron wavelength of 6.0 Å with two sample-to-detector distances to give a combined Q range of 0.01–0.45 $Å^{-1}$. Data were reduced to $I(Q)$ *versus* Q as described previously.[6,33]

Ab initio shape restoration against the X-ray scattering data was performed with DAMMIN.[34] Fifteen independent DAMMIN calculations were performed using the

KipI-dimer data and imposing *P*2 symmetry, all yielding very similar shapes, as determined by the normalized spatial discrepancy factor (0.66 with a mean variation of 0.03). The envelope shown in Fig. 2c is the DAMFILT output by DAMAVER.[35] Rigid-body modeling of the KipI dimer against the X-ray scattering data was performed with SASREF6[36] using PH0987 (PDB entry 2PHC) and imposing *P*2 symmetry. The two-domain PH0987 structure was split between residues 83 and 84, while constraining them to be within 10 Å of each other, so that the N- and C-domains could move independently to account for differences in the sequences linking the domains between the PH0987 and KipI structures.

Rigid-body refinement of the $KinA_2$–2KipI structural model against the neutron data was performed the beads with SASREF7 and imposing *P*2 symmetry. The $KinA_2$ component was that already optimized to fit the $KinA_2$–2^{D}Sda data; based on the crystal structure of the homologous HK853 from *T. maritima* (PDB entry 2C2A). The bound KipI was modeled from the crystal structure of PH0987 with the two domains split as for the X-ray scattering data modeling of the KipI dimer. No constraints were applied on the $KinA^{383–606}$–KipI interaction and all eight neutron contrast measurements were used with a Q range of 0.01–0.25 $Å^{-1}$. Six independent refinements were performed.

Pull-down assays

The $KinA^{383–606}$ or $KinA^{383–606}$(P410L/F436S) was immobilized on 20 μL Ni-NTA beads by mixing the beads with 5.5 nmol His-tagged protein, all in Buffer A. A twofold molar excess of Sda or GST-KipI was subsequently mixed with the beads in a total volume of 320 μL and incubated with mixing at 4 °C for 1 h. Controls in which Sda or GST-KipI alone was mixed with unmodified beads were also performed. The beads were pelleted by centrifugation and, after removal of the supernatant, washed three times with Buffer A. Aliquots of samples containing whole beads were loaded onto 12% SDS-PAGE to evaluate binding interactions.

Tryptophan fluorescence experiments

Fluorescence measurements were performed on a Cary Eclipse Fluorescence Spectrophotometer (Varian Inc.) using an excitation wavelength of 295 nm. Emission spectra (325–370 nm) were collected at 0.5-nm intervals using excitation and emission slit widths of 5 nm. Reported data are the average of three scans recorded at 30 nm/min. KipI (21 μM) was measured in the presence of increasing amounts of $KinA^{383–606}$ (up to 25 μM) or $KinA^{383–606}$(P410L/F436S). Spectra were corrected for buffer and $KinA^{383–606}$ fluorescence.

Crystallography

A single crystal of the C-domain of KipI was obtained by hanging-drop vapour-diffusion, where 2 μL protein (7 mg/mL) was mixed with 2 μL precipitant (15% polyethylene glycol 8000, 20% glycerol, 40 mM potassium phosphate, pH 6.9) at 293 K. The crystal was cryoprotected by swimming it for a few seconds in well solution doped with 2-methyl-2,4-pentanediol (20% v/v) before flash-freezing it in a cold nitrogen stream (100 K, Oxford Cryostream). Diffraction data were recorded on a Marresearch image plate detector using radiation ($\lambda = 1.5418$ Å) from a Rigaku RU200 rotating anode generator fitted with Osmic optics. Data were integrated and scaled with DENZO and SCALEPACK from the HKL suite.[37] Molecular replacement was performed using PHASER,[38] with a trimmed-version of the C-domain from PH0987 (PDB entry 2PHC) as the search model. The structure was refined using REFMAC,[39] manually inspected with COOT,[40] and validated with the MOLPROBITY server,[41] which revealed 88.9% and 1.3% of residues lying in favoured and outlier regions, respectively, of a Ramachandran plot. Data collection and refinement statistics are given in Table 2.

Protein Data Bank accession numbers

Coordinates and structure factors have been deposited in the Protein Data Bank with accession number 2ZP2.

Acknowledgements

We thank Boualem Hammouda for assistance in using neutron scattering facilities, Ben Crossett for performing mass spectrometry, Andrew E. Whitten for helpful advice in the scattering data acquisition and analysis, and Liz Harry for the gift of *B. subtilis* 168 chromosomal DNA. This research was supported by an Australian Research Council Federation Fellowship and U.S. Department of Energy Grant DE-FG02-05ER64026 to J.T. The project also benefitted from support by National Health and Medical Research Council Project Grant 352434 (J. M.G.). D.A.J. is supported by an Australian Institute of Nuclear Science and Engineering Postgraduate Research Award. We acknowledge the support of the National Institute of Standards and Technology (NIST), U.S. Department of Commerce, in providing the neutron research facilities that were supported in part by the National Science Foundation under Agreement No. DMR-0454672. Travel to NIST was supported by the Access to Major Research Facilities Programme (project no. 06/07-N-13). Mass Spectrometry was done using the Australian Proteome Analysis Facility established under the Australian Government's Major National Facilities program.

Supplementary Data

Supplementary data associated with this article can be found, in the online version, at doi:10.1016/j.jmb.2008.09.017

References

1. Hoch, J. A. (2000). Two-component and phosphorelay signal transduction. *Curr. Opin. Microbiol.* **3**, 165–170.
2. Burbulys, D., Trach, K. A. & Hoch, J. A. (1991). Initiation of sporulation in *B. subtilis* is controlled by a multicomponent phosphorelay. *Cell*, **64**, 545–552.

3. Hilbert, D. W. & Piggot, P. J. (2004). Compartmentalization of gene expression during *Bacillus subtilis* spore formation. *Microbiol. Mol. Biol. Rev.* **68**, 234–262.
4. Molle, V., Fujita, M., Jensen, S. T., Eichenberger, P., Gonzalez-Pastor, J. E., Liu, J. S. & Losick, R. (2003). The Spo0A regulon of *Bacillus subtilis*. *Mol. Microbiol.* **50**, 1683–1701.
5. Rowland, S. L., Burkholder, W. F., Cunningham, K. A., Maciejewski, M. W., Grossman, A. D. & King, G. F. (2004). Structure and mechanism of action of Sda, an inhibitor of the histidine kinases that regulate initiation of sporulation in *Bacillus subtilis*. *Mol. Cell*, **13**, 689–701.
6. Whitten, A. E., Jacques, D. A., Hammouda, B., Hanley, T., King, G. F., Guss, J. M. *et al.* (2007). The structure of the KinA–Sda complex suggests an allosteric mechanism of histidine kinase inhibition. *J. Mol. Biol.* **368**, 407–420.
7. Cuff, J. A., Clamp, M. E., Siddiqui, A. S., Finlay, M. & Barton, G. J. (1998). JPred: a consensus secondary structure prediction server. *Bioinformatics*, **14**, 892–893.
8. Wang, L., Fabret, C., Kanamaru, K., Stephenson, K., Dartois, V., Perego, M. & Hoch, J. A. (2001). Dissection of the functional and structural domains of phosphorelay histidine kinase a of *Bacillus subtilis*. *J. Bacteriol.* **183**, 2795–2802.
9. Marina, A., Waldburger, C. D. & Hendrickson, W. A. (2005). Structure of the entire cytoplasmic portion of a sensor histidine-kinase protein. *EMBO J.* **24**, 4247–4259.
10. Perego, M., Glaser, P. & Hoch, J. A. (1996). Aspartyl-phosphate phosphatases deactivate the response regulator components of the sporulation signal transduction system in *Bacillus subtilis*. *Mol. Microbiol.* **19**, 1151–1157.
11. Sonenshein, A. L. (2000). Control of sporulation initiation in *Bacillus subtilis*. *Curr. Opin. Microbiol.* **3**, 561–566.
12. Burkholder, W. F., Kurtser, I. & Grossman, A. D. (2001). Replication initiation proteins regulate a developmental checkpoint in *Bacillus subtilis*. *Cell*, **104**, 269–279.
13. Wang, L., Grau, R., Perego, M. & Hoch, J. A. (1997). A novel histidine kinase inhibitor regulating development in *Bacillus subtilis*. *Genes Dev.* **11**, 2569–2579.
14. Ruvolo, M. V., Mach, K. E. & Burkholder, W. F. (2006). Proteolysis of the replication checkpoint protein Sda is necessary for the efficient initiation of sporulation after transient replication stress in *Bacillus subtilis*. *Mol. Microbiol.* **60**, 1490–1508.
15. Grebe, T. W. & Stock, J. B. (1999). The histidine protein kinase superfamily. *Adv. Microb. Physiol.* **41**, 139–227.
16. Semenyuk, A. V. & Svergun, D. I. (1991). GNOM—a program package for small-angle scattering data-processing. *J. Appl. Crystallogr.* **24**, 537–540.
17. Whitten, A. E., Ca, S. Z. & Trewhella, J. (2008). MULCh: modules for the analysis of small-angle neutron contrast variation data from biomolecular assemblies. *J. Appl. Crystallogr.* **41**, 222–226.
18. Madej, T., Gibrat, J. F. & Bryant, S. H. (1995). Threading a database of protein cores. *Proteins: Struct. Funct. Genet.* **23**, 356–369.
19. Wang, P. & Heitman, J. (2005). The cyclophilins. *Genome Biol.* **6**, 226.
20. Huse, M., Chen, Y. G., Massague, J. & Kuriyan, J. (1999). Crystal structure of the cytoplasmic domain of the type I TGF beta receptor in complex with FKBP12. *Cell*, **96**, 425–436.
21. Ikura, T. & Ito, N. (2007). Requirements for peptidyl-prolyl isomerization activity: a comprehensive mutational analysis of the substrate-binding cavity of FK506-binding protein 12. *Protein Sci.* **16**, 2618–2625.
22. Lombardia, E., Rovetto, A. J., Arabolaza, A. L. & Grau, R. R. (2006). A LuxS-dependent cell-to-cell language regulates social behavior and development in *Bacillus subtilis*. *J. Bacteriol.* **188**, 4442–4452.
23. Tomomori, C., Tanaka, T., Dutta, R., Park, H. Y., Saha, S. K., Zhu, Y. *et al.* (1999). Solution structure of the homodimeric core domain of *Escherichia coli* histidine kinase EnvZ. *Nat. Struct. Biol.* **6**, 729–734.
24. Varughese, K. I., Madhusudan, Zhou, X. Z., Whiteley, J. M. & Hoch, J. A. (1998). Formation of a novel four-helix bundle and molecular recognition sites by dimerization of a response regulator phosphotransferase. *Mol. Cell*, **2**, 485–493.
25. Xavier, K. B. & Bassler, B. L. (2003). LuxS quorum sensing: more than just a numbers game. *Curr. Opin. Microbiol.* **6**, 191–197.
26. Hamon, M. A. & Lazazzera, B. A. (2001). The sporulation transcription factor Spo0A is required for biofilm development in *Bacillus subtilis*. *Mol. Microbiol.* **42**, 1199–1209.
27. Kobayashi, K., Kuwana, R. & Takamatsu, H. (2008). kinA mRNA is missing a stop codon in the undomesticated *Bacillus subtilis* strain ATCC 6051. *Microbiology*, **154**, 54–63.
28. Gasteiger, E., Gattiker, A., Hoogland, C., Ivanyi, I., Appel, R. D. & Bairoch, A. (2003). ExPASy: the proteomics server for in-depth protein knowledge and analysis. *Nucleic Acids Res.* **31**, 3784–3788.
29. Krigbaum, W. R. & Kugler, F. R. (1970). Molecular conformation of egg-white lysozyme and bovine alpha-lactalbumin in solution. *Biochemistry*, **9**, 1216–1223.
30. Orthaber, D., Bergmann, A. & Glatter, O. (2000). SAXS experiments on absolute scale with Kratky systems using water as a secondary standard. *J. Appl. Crystallogr.* **33**, 218–225.
31. Jeffries, C. M., Whitten, A. E., Harris, S. P. & Trewhella, J. (2008). Small-angle X-ray scattering reveals the N-terminal domain organization of cardiac myosin binding protein C. *J. Mol. Biol.* **377**, 1186–1199.
32. Glinka, C. J., Barker, J. G., Hammouda, B., Krueger, S., Moyer, J. J. & Orts, W. J. (1998). The 30 m small-angle neutron scattering instruments at the National Institute of Standards and Technology. *J. Appl. Crystallogr.* **31**, 430–445.
33. Kline, S. R. (2006). Reduction and analysis of SANS and USANS data using IGOR Pro. *J. Appl. Crystallogr.* **39**, 895–900.
34. Svergun, D. I. (1999). Restoring low resolution structure of biological macromolecules from solution scattering using simulated annealing. *Biophys. J.* **76**, 2879–2886.
35. Volkov, V. V. & Svergun, D. I. (2003). Uniqueness of ab initio shape determination in small-angle scattering. *J. Appl. Crystallogr.* **36**, 860–864.
36. Petoukhov, M. V. & Svergun, D. I. (2005). Global rigid body modeling of macromolecular complexes against small-angle scattering data. *Biophys. J.* **89**, 1237–1250.
37. Otwinowski, Z. & Minor, W. (1997). Processing of X-ray diffraction data collected in oscillation mode. *Macromol. Crystallogr.* **276**, 307–326.
38. McCoy, A. J., Grosse-Kunstleve, R. W., Adams, P. D., Winn, M. D., Storoni, L. C. & Read, R. J. (2007). Phaser

crystallographic software. *J. Appl. Crystallogr.* **40**, 658–674.
39. Murshudov, G. N., Vagin, A. A. & Dodson, E. J. (1997). Refinement of macromolecular structures by the maximum-likelihood method. *Acta Crystallogr., Sect. D: Biol. Crystallogr.* **53**, 240–255.
40. Emsley, P. & Cowtan, K. (2004). Coot: model-building tools for molecular graphics. *Acta Crystallogr., Sect. D: Biol. Crystallogr.* **60**, 2126–2132.
41. Davis, I. W., Leaver-Fay, A., Chen, V. B., Block, J. N., Kapral, G. J., Wang, X. *et al.* (2007). MolProbity: all-atom contacts and structure validation for proteins and nucleic acids. *Nucleic Acids Res.* **35**, W375–W383.